

Tailoring the electrical properties of tellurium nanowires via surface charge transfer doping

Lin-Bao Luo · Feng-Xia Liang · Xiao-Li Huang · Tian-Xin Yan · Ji-Gang Hu ·
Yong-Qiang Yu · Chun-Yan Wu · Li Wang · Zhi-Feng Zhu · Qiang Li ·
Jian-Sheng Jie

Received: 3 February 2012 / Accepted: 30 May 2012 / Published online: 10 June 2012
© Springer Science+Business Media B.V. 2012

Abstract We presented an attempt to modulate the electrical property of tellurium nanowires (TeNWs) via a surface charge transfer doping method. The TeNWs with length of several tens of micrometers and diameters of 20–50 nm were prepared by a simple hydrothermal method at 160 °C for 20 h. High-resolution transmission electron microscope image combined with selected area electron diffraction pattern shows the single-crystal nature and a growth direction along [001]. Electrical analysis of the individual TeNW-based field effect transistor before and after surface coating reveals that MoO₃ and CuPc thin layer coating can greatly enhance both electrical conductivities and hole concentrations. Such a surface hole injection effect, according to the band energy

alignment, can be attributed to the huge differences in work functions between TeNW and MoO₃/CuPc. Furthermore, the influence of the deposited layer on carrier mobility is strikingly different, which is believed to be due to the discrepancy in surface scattering upon surface coating. The results from this study provide an effective alternative for doping other semiconductor nanostructures.

Keywords Tellurium nanowires · Charge transfer doping · Electrical property · Hole injection

Introduction

One-dimensional (1-D) nanoscaled semiconductor materials, such as nanotubes, nanowires, and nanoribbons, have attracted great research interest due to their high crystallinity, huge surface-to-volume ratio, enhanced electrical and optical properties relative to their thin film, and bulk counterparts (Hochbaum and Yang 2010; Huang et al. 2001a, b; Luo et al. 2009; Wu et al. 2011). A variety of methods have been reported thus far to synthesize 1-D nanostructures from elements to compounds, in an effort to develop novel and high-performance electronic and optoelectronic nanodevices including field effect transistors (FETs), biological and chemical sensors, visible or UV light

L.-B. Luo (✉) · X.-L. Huang · T.-X. Yan ·
J.-G. Hu · Y.-Q. Yu · C.-Y. Wu · L. Wang ·
Z.-F. Zhu · Q. Li · J.-S. Jie (✉)
School of Electronic Science and Applied Physics,
Hefei University of Technology, Hefei, Anhui 230009,
People's Republic of China
e-mail: luolb@hfut.edu.cn

J.-S. Jie
e-mail: jsjie@hfut.edu.cn

F.-X. Liang
Department of Physics and Materials Science,
City University of Hong Kong, Hong Kong SAR,
People's Republic of China

photodetectors, and solar cells (Morales and Lieber 1998; Xia et al. 2003). 1-D semiconductor nanostructures are considered the most promising candidate of building blocks for constructing powerful electronic devices.

Tellurium in trigonal phase is a typical *p*-type narrow gap elementary semiconductor, with a direct band gap of 0.35 eV at room temperature (Kudrjavcev 1974). Single-crystalline nanostructured tellurium, especially in 1-D form, has garnered extensive attention lately because of their promising potential for constructing high-performance optoelectronic devices such as visible light photodetectors (Liu et al. 2009) and nano FET (Liang and Qian 2009). To date, various methods have been developed to prepare 1-D tellurium nanostructures. Xia et al. have reported the fabrication of 1-D nanostructure of *t*-Te via a solution phase procedure (Mayers and Xia 2002). Gautam's group developed a hydrothermal route to prepare Y-junction NWs in the presence of a strong reducing reagent, NaBH₄ (Gautam and Rao 2004). Furthermore, alginate acid, a straight-chain polyuronic acid made of monosaccharide units, was utilized for the synthesis of tellurium nanowires (TeNWs) (Lu et al. 2005). Despite these considerable efforts on the growth, a study on TeNW-based device (e.g. light emitting diode—LED) has rarely been initiated. This difficulty is partially associated with the failure to effectively modulate the electrical property of TeNWs. It is well known that the operation of semiconductor-based electronic devices mainly relies on the density of free charge carriers available in the semiconductor (Huang et al. 2001a, b; Gillissen and Schairer 1987). In most cases, doping is achieved by directly incorporating impurity atoms into the host lattice at high temperature (He et al. 2009), which is practical and widely adopted in semiconductor industry (Bjork et al. 2009; Lu and Lieber 2002; Sze and Ng 2007). However, when comes to tailoring the electrical property of tellurium at nanoscale level, this traditional doping technique is out of place, in that TeNWs are extremely unstable at high temperature (Lan et al. 2007). In this study, we present a novel surface charge transfer doping approach, via which the electrical property of TeNWs can be tuned by surface engineering. It was found that when a thin layer of MoO₃ or CuPc was deposited onto the TeNWs surface, both conductivity and hole concentration of the TeNWs increase considerably. The reason

accounting for this charge transfer at the interface was elucidated at last.

Experiment

Synthesis and structural characterization of TeNWs

The TeNWs were grown through a modified hydrothermal method (Qian et al. 2006a, b). Briefly, 0.5 mmol sodium telluride (Na₂TeO₃, Sigma-Aldrich Co., analytical grade) was dissolved in 25 ml of deionized water, then 1 mmol sodium thiosulphate (Na₂S₂O₃, Sigma-Aldrich Co., analytical grade) was added into the solution. After being vigorously stirred for 30 min, the mixed solution was transferred to a Teflon-lined autoclave with a capacity of 30 ml and heated up to 160 °C for 20 h, then allowed to cool to ambient temperature. The silver colored wool-like product was collected and washed for several times with distilled water and absolute ethanol. The morphology, crystal structure, and chemical composition of TeNWs were characterized by X-ray diffraction (XRD), scanning electron microscopy (SEM, Philips XL 30 FEG) attached with a energy-dispersive X-ray spectroscopy (EDS), transmission electron microscopy (TEM, CM 20, operated at 200 kV), and high-resolution transmission electron microscopy (HRTEM, CM 200 FEG, operated at 200 kV). X-ray photoelectron spectroscopy (XPS) analysis was performed on a VG ESCALAB 3 spectrometer, using a monochromatic Al K_α source (1486.6 eV) at a base pressure of less than 10⁻⁹ Torr. Ultraviolet photoemission spectroscopy (UPS) measurements with a total instrumental energy resolution of 90 meV was performed to characterize the energy level of pure TeNWs.

Device fabrication and analysis

The construction of TeNWs-based FET follows a standard process including nanowires dispersion, patterning by photolithography, electrode film deposition by electron-beam evaporator, and finally lift-off (Luo et al. 2012; Patolsky et al. 2006). Briefly, the as-synthesized TeNWs was firstly immersed into an absolute alcohol solution via ultrasonication. The resultant NW suspension was then spread onto a

thermally oxidized p^+ -Si substrate (SiO_2 : 500 nm) by a micropipette (note that each dispersion consumes $\sim 100 \mu\text{l}$ in average). To maximum the number of individual TeNW-based FET devices, the ratio of TeNWs/alcohol was optimized. It is found that the suspension containing 2 mg TeNWs and 15 ml alcohol will lead to most desired TeNWs density on the substrate. After evaporation of the solvent, shadow mask and electron-beam evaporator were utilized to define both source and drain electrodes. Metal deposition was carried out in an ultrahigh-vacuum electron-beam evaporator at a base pressure of 5×10^{-8} Torr. After the fabrication of TeNW-FETs, MoO_3 and CuPc were directly deposited on the device in a thermal evaporator (Edwards, Auto 306). Note that both evaporators mentioned here were equipped with a thickness monitor to control the thickness accurately. The electrical analysis of the TeNW-FETs was performed on a semiconductor I - V characterization system (4200-SCS, Keithley Company) with picoampere sensitivity.

Results and discussion

After synthesis, the crystallinity and purity (phase and composition) of the product was firstly studied by XRD. Figure 1a shows a typical X-ray powder diffraction pattern of the sample obtained. Very clearly, all peaks can be readily indexed to hexagonal phase of tellurium (t -Te), with calculated lattice parameter of $a = 4.46 \text{ \AA}$, $c = 5.92 \text{ \AA}$, in good agreement with the standard date (JCPDF Card number: 36-1452) (Wang et al. 2007). The SEM image at low magnification shown in Fig. 1b indicates that the product is largely composed of wire-like fibers, and no obvious impurity and contaminant are visualized. The fibers are up to several tens of micrometers in length. The yield of these TeNW product was more than 90 %. Figure 1c shows a TEM image of two TeNWs with diameters of ~ 20 and 50 nm. Corresponding EDX analysis of these NWs shows the presence of only tellurium element (the copper signal can be attributed to Cu TEM grid). HRTEM was carried out to unveil the growth direction of the TeNWs, as shown in Fig. 1d, the fringe spacing of the crystal plane perpendicular to the length of the TeNWs is 0.592 nm, corresponding to (001) planes of trigonal Te. Corresponding SAED pattern in the bottom inset of Fig. 1d

confirms the single-crystal nature and [001] orientation of the TeNWs (Qian et al. 2006a, b). This growth direction is in fact consistent with the inherent helical chain of t -Te (Xie et al. 2006).

In order to study the transport properties of the as-prepared TeNWs and further extensively investigate the charge doping effect via surface coating, formation of good contact (*Ohmic* contact) between the TeNWs and electrode metal is a necessity. To this end, we tried many metals such as Ti, Ti/Au, Pt, and Au, and concluded that gold is the most appropriate material to minimize the contact resistance. As displayed in Fig. 2a, a long TeNW was connected by four parallel Au electrodes spaced about $2 \mu\text{m}$ apart. The contact resistance between the semiconductor and metal (R_{con}) and the NW resistance were estimated using the formula of $R^{bc} = R_{\text{nw}}^{bc} + 2R_{\text{con}} + 2R_{\text{ele}}$, where R_{nw}^{bc} and R^{bc} are the resistance measured by four- and two-probe measurements, respectively, and R_{ele} is the resistance of electrode metal, which can be neglected in our case. The resistance R_{nw}^{bc} (between b and c , red line) is calculated to be about 0.7308Ω by fitting the linear part near the 0 V. Additionally, the contact resistance is about $1.78 \times 10^{-3} \Omega$, which is about 0.24 % that of the TeNW resistance. In this connection, two-probe configuration was employed in the following study.

To compare the electrical characteristics of these TeNWs before and after surface deposition, individual TeNW-FETs were fabricated. The inseting diagram in Fig. 3a shows a typical TeNW-FET configuration after surface coating. The gate voltage was applied to the p -type silicon substrate in a global back gate configuration. Figure 3a plots the I - V measurement of pure MoO_3 thin film, pure TeNW, and TeNW covered with MoO_3 . Apparently, after the deposition of the MoO_3 layer, the resistance of the TeNW decrease considerably from 5.0×10^5 to $2.6 \times 10^5 \Omega$. Without question, such an increase in conductivity cannot be ascribed to contribution from deposited thin layer in that the resistance of pure MoO_3 layer is approximately $10^{10} \Omega$, virtually being electrically insulating. As we will discuss later, the surface charge transfer at the MoO_3 and TeNW interface is responsible for the decrease in resistance. In this study, we measured 10 TeNWs in total and the majority of the NWs exhibited increased conductance after surface engineering (cf. Fig. 3b). In addition to MoO_3 , CuPc coating can also reduce resistance of TeNW. As shown in Fig. 3c,

Fig. 1 **a** XRD pattern of the as-prepared TeNWs. **b** A typical SEM image of the TeNWs at low magnification. **c** A typical TEM image of the TeNWs, the *bottom inset* is the corresponding EDS spectrum. **d** HRTEM image of an individual TeNW, the *bottom inset* is the corresponding SAED pattern

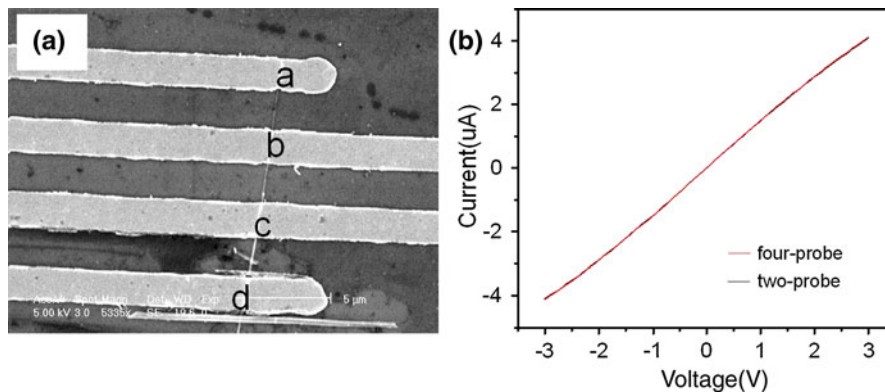
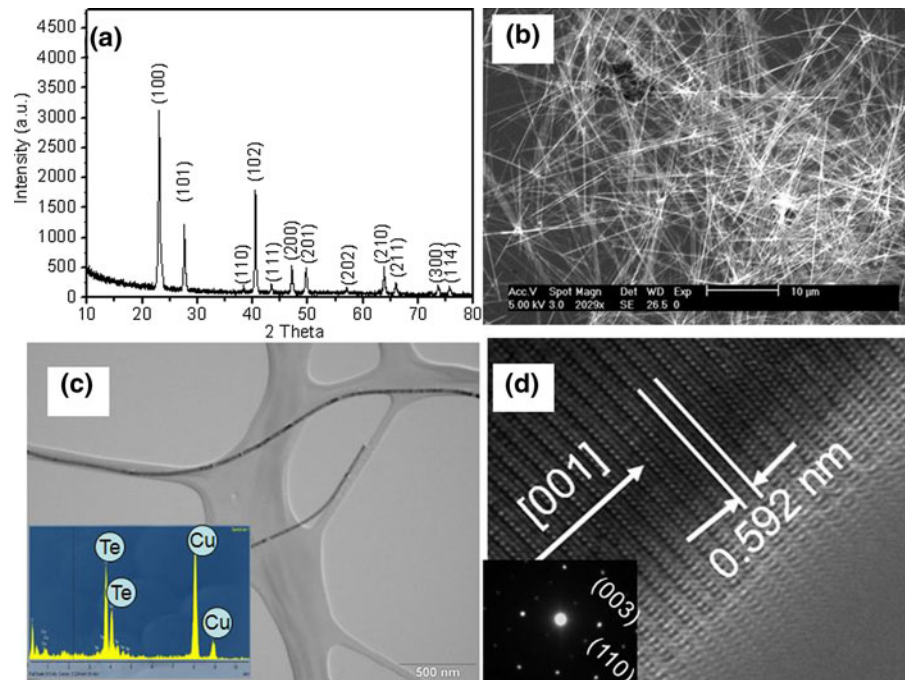


Fig. 2 **a** SEM image of the TeNW connected by four parallel Au electrodes, the four parallel electrodes are marked as *a, b, c, d* from up to down. **b** I - V curves from two- and four-probe measurements

the resistance was found to decrease by nearly 15 times after the CuPc coverage.

Figure 4a shows I_{ds} vs. V_{ds} curves of a typical FET fabricated from a single-naked TeNW at different gate voltages. It was found that when V_g increases (or decreases), the conductance of the TeNW decreases (or increases) accordingly. Such gate-dependent I_{ds} - V_{ds} characteristics signify the p -type conductivity of TeNW. Figure 4b shows the typical transfer characteristics, namely I_{ds} vs. V_{gs} curves at a constant

V_{ds} of -0.06 V. By deducing from the linearly extrapolated value at the V_g axis, a threshold voltage (V_T) of -30 V is obtained. Assuming a cylinder on an infinite plate model for the TeNW-FET, the channel capacitance of the back gate was estimated to be 0.34 fF using the relation of $C = 2\pi\epsilon_0\epsilon_r L / \ln(4h/d)$, where ϵ_0 and ϵ_r is the vacuum permittivity (8.85×10^{-14} F cm $^{-1}$) and effective dielectric constant of SiO $_2$ (3.9), respectively, h (300 nm) the thickness of the dielectric layer, L (5×10^{-4} cm) the channel

Fig. 3 **a** I - V curve of the MoO_3 , pure TeNW, and TeNW with MoO_3 coating, *inset* in **(a)** shows schematic illustration of TeNW-FET with MoO_3 layer. **c** I - V curve of the CuPc, pure TeNW, and TeNW with CuPc coverage. Histograms for I/I_0 with MoO_3 **(b)** and CuPc **(d)** coverage, I/I_0 is defined as the current ratio of TeNW after surface coating to pure TeNW

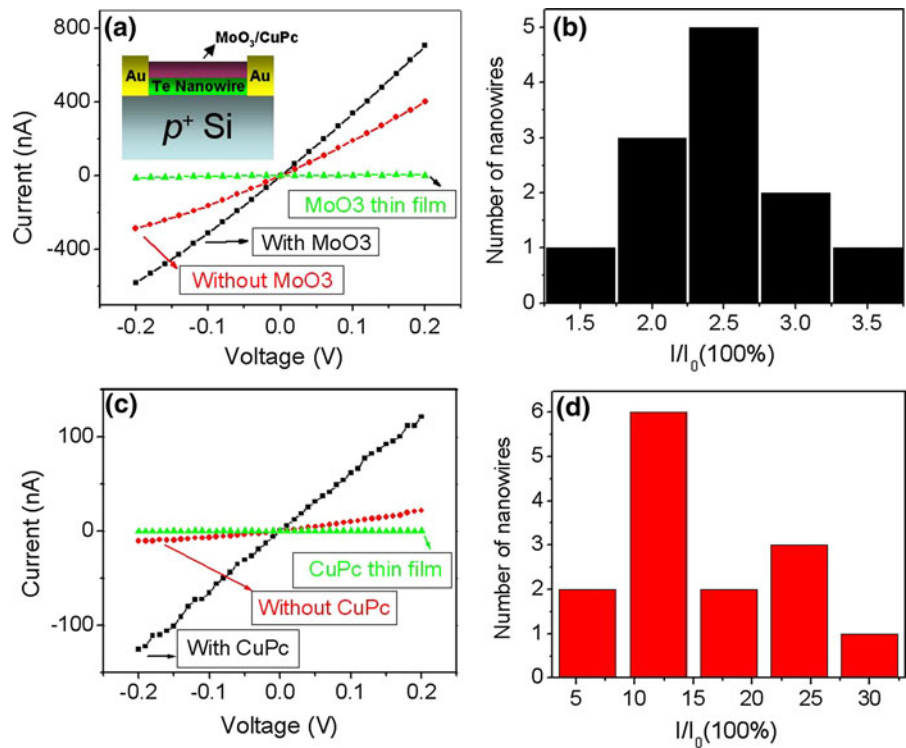
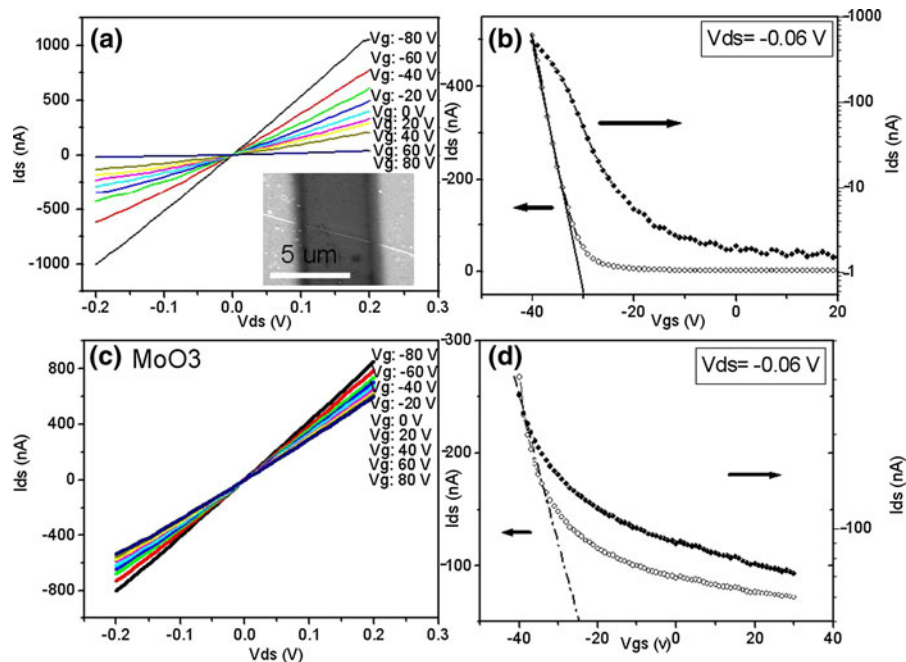


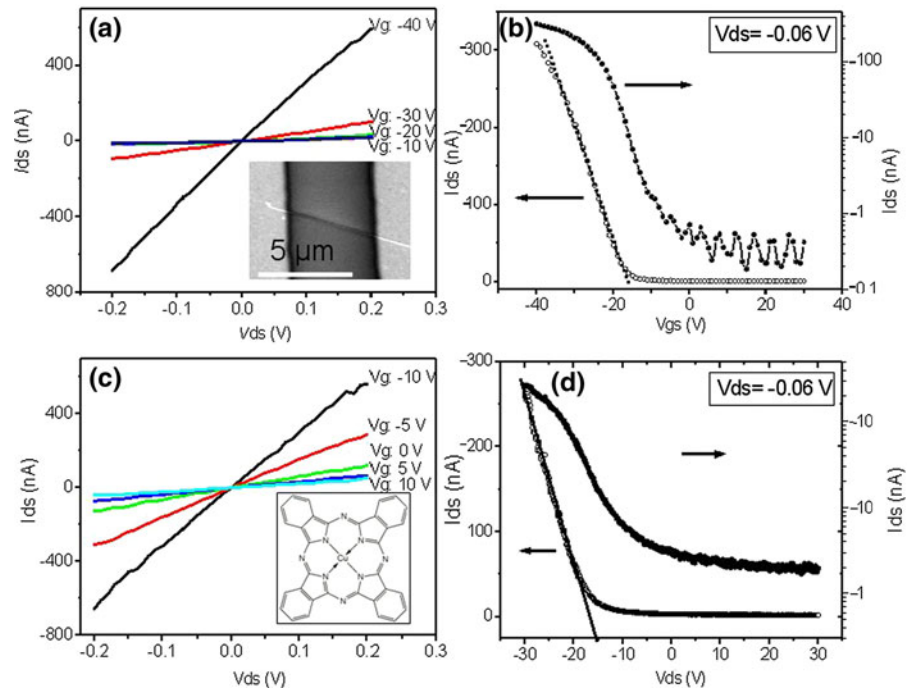
Fig. 4 Electrical characteristics of TeNW-FET device: typical I_{ds} vs. V_{ds} curves at different V_{gs} without MoO_3 **(a)** and with MoO_3 coating **(c)**, the *inset* in **(a)** shows a typical SEM image of a FET device after MoO_3 coating. I_{ds} - V_{gs} recorded at $V_{ds} = -0.06$ V without MoO_3 **(b)** and with MoO_3 coating **(d)**, I_{ds} is shown in both linear (*left*) and logarithmic (*right*) plots



length, and d (5×10^{-6} cm) the radius of the TeNW. The hole mobility (μ_h) can be calculated to be $685 \text{ cm}^2/\text{Vs}$ in the linear operation region using the equation $\mu_h = g_m L^2 / CV_{ds}$, where g_m is given by

$g_m = dI_{ds} / dV_{gs}$, which is about 55.87 nS by fitting the linear part of the curve, and V_{ds} (-0.06 V) is the source drain voltage. Such a mobility is about 2–3 times that of TeNW-based FET (Tao et al. 2003).

Fig. 5 Electrical characteristics of TeNW-FET device: typical I_{ds} vs. V_{ds} curves at different V_{gs} without CuPc (a) and with CuPc coating (c), the *inset* in (a) shows a typical SEM image of a FET device after CuPc coating, and the *bottom inset* in (c) shows the molecular structure of CuPc. I_{ds} - V_{gs} recorded at $V_{ds} = -0.06$ V without CuPc (b) and with CuPc coating (d), I_{ds} is shown in both linear (*left*) and logarithmic (*right*) plots



Additionally, the hole concentration is determined to be $4.26 \times 10^{17} \text{ cm}^{-3}$ from the formula of $\rho = 1/n_h q \mu_h$. Significantly, upon deposition of MoO_3 layer with thickness around 30 nm, a striking change in electrical property of TeNW-FET was observed. Figure 4c and d plots the I_{ds} - V_{ds} curves at different V_g and the transfer characteristics at $V_{ds} = -0.06$ V, respectively. The carrier mobility is determined to be $155 \text{ cm}^2/\text{Vs}$, slightly lower than that of pure TeNW-FET. What is more, the calculated hole concentration is $3.32 \times 10^{18} \text{ cm}^{-3}$, nearly one order of magnitude larger than that of pure TeNW-FET.

Similar doping effect was observed on CuPc thin film as well. Figure 5 compares the transport properties of another TeNWs at different conditions. Clearly, prior to CuPc coating, the TeNW exhibits a *p*-type electrical conduction, with a hole mobility of $172 \text{ cm}^2/\text{Vs}$ and hole concentration of $7.58 \times 10^{16} \text{ cm}^{-3}$, respectively. But, deposition of a layer of 30 nm thick

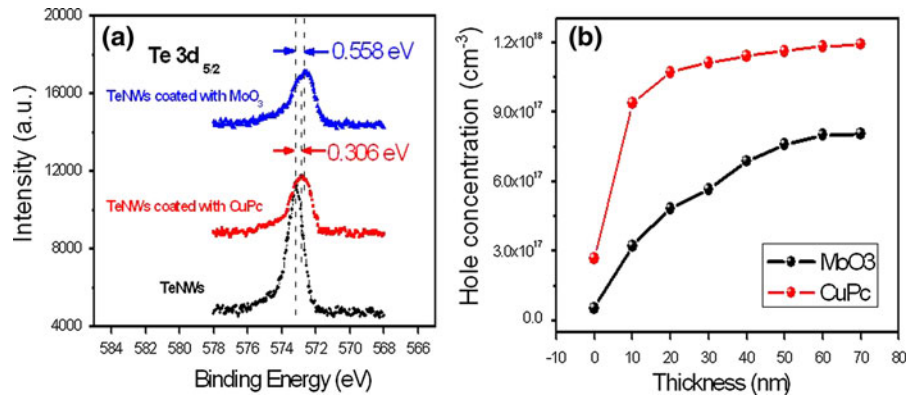
CuPc can lead to a pronounced increase in hole concentration ($4.27 \times 10^{17} \text{ cm}^{-3}$). Meanwhile, the carrier mobility increases a little bit to $231 \text{ cm}^2/\text{Vs}$, which is different from that with MoO_3 coating. The change of carrier mobility, hole concentration, threshold voltage, and on/off ratio of the TeNW-FET device before and after surface coating was summarized in Table 1.

Though both MoO_3 and CuPc thin film deposition can improve the hole concentration and electrical conduction of the TeNWs, nevertheless it is worth noting that their influences on the carrier mobility are opposite. This discrepancy is probably associated with the surface scattering effect, as a result of surface passivation or termination. Previously, it has been observed on silicon NWs that due to the huge surface-to-volume ratio, the surface defect including surface dangling bond, surface adsorbents species can influence the transport properties. Generally, the stronger

Table 1 Comparison of carrier mobility, hole concentration, threshold voltage, and on/off ratio of TeNW without and with the coverage of MoO_3 and CuPc layer

	Carrier mobility (cm^2/Vs)	Hole concentration (cm^{-3})	Threshold voltage (V)	On/off ratio
TeNW/ MoO_3 @TeNW	685/155	$4.26 \times 10^{17}/3.32 \times 10^{18}$	-30/-25	500/3
TeNW/CuPc@TeNW	172/231	$7.58 \times 10^{16}/4.27 \times 10^{17}$	-15/-15	1000/1000

Fig. 6 **a** XPS spectra of Te3d peaks for pure TeNWs, TeNWs coated with 10 nm MoO₃ layer, and TeNWs coated with 10 nm CuPc layer. **b** Hole concentration vs. the thickness of the MoO₃/CuPc layer

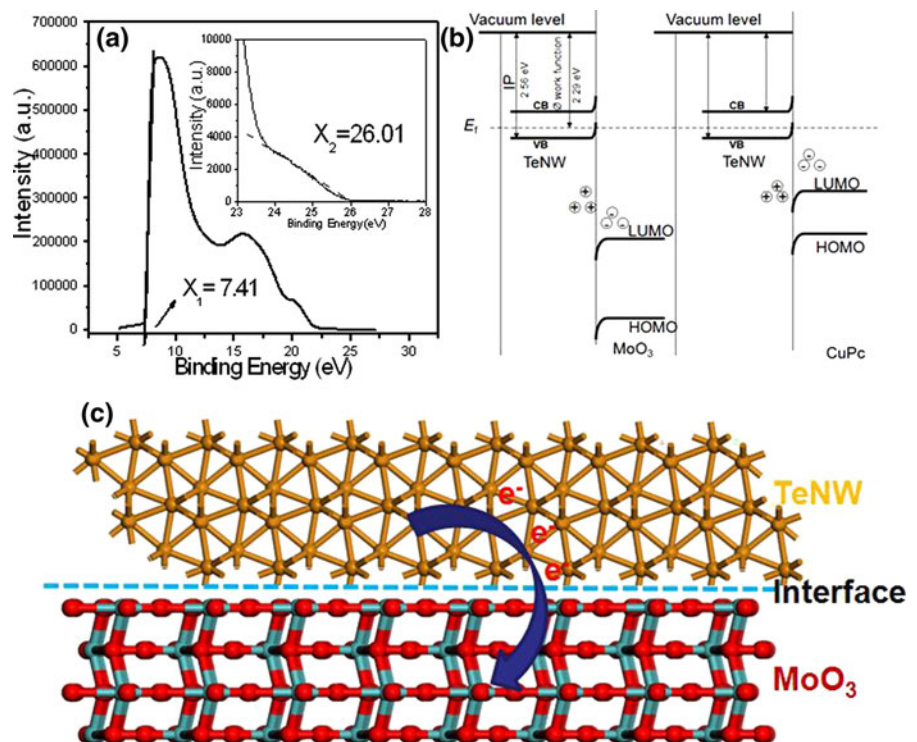


the surface scattering effect of surface defects on carriers, the lower the carrier mobility would be (Schmidt et al. 2009). In light of this, the MoO₃ deposition induced decrease in hole mobility can be ascribed to the increase in surface scattering after surface coating, whereas for CuPc, the increased mobility can be, in contrast, attributed to decrease in surface scattering when CuPc layer was coated. The exact reason for this phenomenon is still unknown to us and need further investigation.

The enhancement of hole concentration was further verified by interface charge transfer between TeNW

and MoO₃/CuPc by XPS analysis. As shown in Fig. 6a, the XPS spectrum of pure TeNWs shows a Te3d peak at 573.218 eV. After surface deposition of MoO₃ and CuPc, the binding energy shifts to 572.892 and 572.660 eV, respectively. These shifts to lower binding energy indicate an upward band bending at the TeNW surface region, which was induced by hole accumulation at TeNW to balance the negatively charged molecules (Qi et al. 2007; Yuan et al. 2010). The weakened signal after surface coating is understandable considering the fact that the thickness of deposited layer is larger than the effective analysis

Fig. 7 **a** UPS spectrum of TeNWs. **b** Electronic structures diagram of the TeNW and MoO₃/CuPc. **c** Schematic illustration of the electron injection from TeNW to MoO₃



depth of the instrument, which is normally 5–10 nm. To further study the controllability of this surface doping method, the hole concentration evolution as a function of layer thickness was carried out. The black line in Fig. 6b depicted the hole concentration corresponding to increasing thickness of MoO₃ layer. When 10 nm thick MoO₃ was coated, the hole increase from 5.37×10^{16} to 3.21×10^{17} . As the thickness further increases to 20, 30, 40, 50, and 60 nm, the hole concentration increases to 4.83×10^{17} , 5.65×10^{17} , 6.86×10^{17} , 7.59×10^{17} , and $7.98 \times 10^{17} \text{ cm}^{-3}$, respectively. Similar hole concentration dependence on CuPc was observed as well. Nevertheless, when the thickness reached 60 nm (MoO₃) or 40 nm (CuPc), the hole concentration reached a constant, independent of further increase of the dopant layer. This saturation in hole concentration suggests that only the dopant layer near the TeNW interface contribute to the charge transfer.

To elucidate the physical origin of hole concentration enhancement by MoO₃/CuPc thin layer deposition, we compared the energy level diagram of the TeNW and MoO₃/CuPc. The UPS spectra of pure TeNWs were shown in Fig. 7a, from which, two cutoff values ($X_1 = 7.41 \text{ eV}$ and $X_2 = 26.01 \text{ eV}$) at low- and high-binding energy were derived. Based on these two values, the ionization potential (IP) and fermi level (Φ) are estimated to be 2.29 and 2.56 eV, respectively. Figure 7b aligns the energy levels of both TeNW/MoO₃ and TeNW/CuPc interfaces. The lowest unoccupied molecular orbital (LUMO) value of $-6.7/-3.4 \text{ eV}$ and highest occupied molecular orbital (HOMO) value of $-9.7/-5.2 \text{ eV}$ of MoO₃/CuPc are lower than that of TeNWs (Kröger et al. 2009; Ng et al. 2009). This feature suggests that the Fermi level of TeNWs is higher than that of MoO₃ and CuPc, thus it facilitates the spontaneous electron transfer from TeNW to MoO₃/CuPc.

Conclusion

In summary, we reported on the surface transfer *p*-type doping of TeNWs via thin layer deposition. The single [001] oriented TeNWs were synthesized by a simple hydrothermal method. Electrical property analysis shows that both electrical conductance and hole concentration are prominently enhanced after MoO₃/CuPc coating. Such a remarkable surface doping effect

is due to the surface charge transfer, as a result of the huge difference of work functions between TeNW and MoO₃/CuPc. These results suggest that surface charge transfer doping is an effective method to modulate the electrical property of TeNWs.

Acknowledgments The authors thank Dr. Hong-Bing Yao at University of Science and Technology of China for generous help and constructive discussion. This work was supported by the National Natural Science Foundation of China (Nos. 60806028, 61106010, 21101051, and 20901021), the Program for New Century Excellent Talents in University of the Chinese Ministry of Education (NCET-08-0764), the Major Research Plan of the National Natural Science Foundation of China (No. 91027021), and the Fundamental Research Funds for the Central Universities.

References

- Bjork M, Schmid H, Knoch J, Riel H, Riess W (2009) Donor deactivation in silicon nanostructures. *Nat Nanotechnol* 4:103–107. doi:[10.1038/nnano.2008.400](https://doi.org/10.1038/nnano.2008.400)
- Gautam U, Rao C (2004) Controlled synthesis of crystalline tellurium nanorods, nanowires, nanobelts and related structures by a self-seeding solution process. *J Mater Chem* 14:2530–2535. doi:[10.1039/B405006A](https://doi.org/10.1039/B405006A)
- Gillessen K, Schairer W (1987) *Light emitting diodes: an introduction*. Prentice Hall International, London
- He Z, Jie J, Zhang W, Luo L, Fan X, Yuan G, Bello I, Lee S (2009) Tuning electrical and photoelectrical properties of CdSe nanowires via indium doping. *Small* 5:345–350. doi:[10.1002/sml.200801006](https://doi.org/10.1002/sml.200801006)
- Hochbaum A, Yang P (2010) Semiconductor nanowires for energy conversion. *Chem Rev* 110:527–546. doi:[10.1021/cr900075v](https://doi.org/10.1021/cr900075v)
- Huang M, Mao S, Feick H, Yan H, Wu Y, Kind H, Weber E, Russo R, Yang P (2001a) Room-temperature ultraviolet nanowire nanolasers. *Science* 292:1897–1899. doi:[10.1126/science.1060367](https://doi.org/10.1126/science.1060367)
- Huang Y, Duan X, Cui Y, Lathon L, Kim K, Lieber C (2001b) Logic gates and computation from assembled nanowire building blocks. *Science* 294:1313–1317. doi:[10.1126/science.1066192](https://doi.org/10.1126/science.1066192)
- Kröger M, Hamwi S, Meyer J, Riedl T, Kowalsky W, Kahn A (2009) *P*-type doping of organic wide band gap materials by transition metal oxides: a case-study on molybdenum trioxide. *Org Electron* 10:932–938. doi:[10.1016/j.orgel.2009.05.007](https://doi.org/10.1016/j.orgel.2009.05.007)
- Kudrjavcev A (1974) *The chemistry and technology of selenium and tellurium*. Collet's, London
- Lan W, Yu S, Qian H, Wan Y (2007) Dispersibility, stabilization, and chemical stability of ultrathin tellurium nanowires in acetone: morphology change, crystallization, and transformation into TeO₂ in different solvents. *Langmuir* 23:3409–3417. doi:[10.1021/la063272+](https://doi.org/10.1021/la063272+)
- Liang F, Qian H (2009) Synthesis of tellurium nanowires and their transport property. *Mater Chem Phys* 113:523–526. doi:[10.1016/j.matchemphys.2008.07.101](https://doi.org/10.1016/j.matchemphys.2008.07.101)

- Liu J, Zhu J, Zhang C, Liang H, Yu S (2009) Mesostructured assemblies of ultrathin superlong tellurium nanowires and their photoconductivity. *J Am Chem Soc* 132:8945–8952. doi:[10.1021/ja910871s](https://doi.org/10.1021/ja910871s)
- Lu W, Lieber C (2002) Nanoelectronics from the bottom up. *Nat Mater* 6:841–850. doi:[10.1038/nmat2028](https://doi.org/10.1038/nmat2028)
- Lu Q, Gao F, Komarneni S (2005) A green chemical approach to the synthesis of tellurium nanowires. *Langmuir* 16:6002–6005. doi:[10.1021/la050594p](https://doi.org/10.1021/la050594p)
- Luo L, Jie J, Zhang W, He Z, Wang J, Yuan G, Zhang W, Wu C, Lee S (2009) Silicon nanowire sensors for Hg^{2+} and Cd^{2+} ions. *Appl Phys Lett* 94:193101. doi:[10.1063/1.3120281](https://doi.org/10.1063/1.3120281)
- Luo L, Yang X, Liang F, Jie J, Li Q, Zhu ZF, Wu CY, Yu Y, Wang L (2012) Transparent and flexible selenium nanobelt-based visible light photodetector. *CrystEngComm* 14:1942–1947. doi:[10.1039/c2ra01269c](https://doi.org/10.1039/c2ra01269c)
- Mayers B, Xia Y (2002) Formation of tellurium nanotubes through concentration depletion at the surfaces of seeds. *Adv Mater* 14:279–282. doi:[10.1002/1521-4095\(20020219\)14:279::AID-ADMA20020219](https://doi.org/10.1002/1521-4095(20020219)14:279::AID-ADMA20020219)
- Morales A, Lieber C (1998) A laser ablation method for the synthesis of crystalline semiconductor nanowires. *Science* 279:208–211. doi:[10.1126/science.279.5348.208](https://doi.org/10.1126/science.279.5348.208)
- Ng T, Lo M, Zhou Y, Liu Z, Lee C, Kwon O, Lee S (2009) Ambient effects on fullerene/copper phthalocyanine photovoltaic interface. *Appl Phys Lett* 94:193304. doi:[10.1063/1.3118580](https://doi.org/10.1063/1.3118580)
- Patolsky F, Zheng G, Lieber C (2006) Fabrication of silicon nanowire devices for ultrasensitive, label-free, real-time detection of biological and chemical species. *Nat Protoc* 1:1711–1724. doi:[10.1038/nprot.2006.227](https://doi.org/10.1038/nprot.2006.227)
- Qi D, Chen W, Gao X, Wang L, Chen S, Loh KP, Wee ATS (2007) Surface transfer doping of diamond (100) by tetrafluoro-tetracyanoquinodimethane. *J Am Chem Soc* 129:8084–8085. doi:[10.1021/ja072133r](https://doi.org/10.1021/ja072133r)
- Qian H, Luo L, Gong J, Yu S, Fei L (2006a) Te@cross-linked PVA core-shell structures synthesized by a one-step synergistic soft-hard template process. *Cryst Growth Des* 18:2102–2108. doi:[10.1021/cg050412p](https://doi.org/10.1021/cg050412p)
- Qian H, Yu S, Gong J, Luo L, Fei L (2006b) High-quality luminescent tellurium nanowires of several nanometers in diameter and high aspect ratio synthesized by a poly (vinyl pyrrolidone)-assisted hydrothermal process. *Langmuir* 22:3830–3835. doi:[10.1021/la0530211](https://doi.org/10.1021/la0530211)
- Schmidt V, Wittemann JV, Senz S, Gösele U (2009) Silicon nanowires: a review on aspects of their growth and their electrical properties. *Adv Mater* 21:2681–2702. doi:[10.1002/adma.200803754](https://doi.org/10.1002/adma.200803754)
- Sze S, Ng K (2007) *Physics of semiconductor devices*. Wiley-Blackwell, Boston, MA
- Tao H, Liu H, Qin D, Chan K, Chen J, Cao Y (2003) High mobility field effect transistors from solution-processed needle-like tellurium nanowires. *J Nanosci Nanotechnol* 10:7997–8003. doi:[10.1166/jnn.2010.3000](https://doi.org/10.1166/jnn.2010.3000)
- Wang Q, Li G, Liu Y, Xu S, Wang K, Chen J (2007) Fabrication and growth mechanism of selenium and tellurium nanobelts through a vacuum vapor deposition route. *J Phys Chem C* 111:12926–12932. doi:[10.1021/jp073902w](https://doi.org/10.1021/jp073902w)
- Wu D, Jiang Y, Li S, Li F, Li J, Lan X, Zhang Y, Wu C, Luo L, Jie J (2011) Construction of high-quality CdS:Ga nanoribbon/silicon heterojunctions and their nano-optoelectronic applications. *Nanotechnology* 22:405201. doi:[10.1088/0957-4484/22/40/405201](https://doi.org/10.1088/0957-4484/22/40/405201)
- Xia Y, Yang P, Sun G, Wu Y, Mayers B, Gates B, Yin Y, Kim F, Yan H (2003) One-dimensional nanostructures: synthesis, characterization, and applications. *Adv Mater* 15:353–389. doi:[10.1002/adma.200390087](https://doi.org/10.1002/adma.200390087)
- Xie Q, Zhou D, Huang W, Zhang W, Ma D, Hu X, Qian Y (2006) Large-scale synthesis and growth mechanism of single-crystal Se nanobelts. *Cryst Growth Des* 6:1514–1517. doi:[10.1021/cg050493p](https://doi.org/10.1021/cg050493p)
- Yuan G, Ng T, Zhou Y, Wang F, Zhang W, Tang Y, Tang H, Luo L, Wang P, Bello I (2010) p-type conductivity in silicon nanowires induced by heterojunction interface charge transfer. *Appl Phys Lett* 97:153126. doi:[10.1063/1.3501122](https://doi.org/10.1063/1.3501122)